Climatology of Cyclogenesis over the East China Sea

HOWARD P. HANSON

Cooperative Institute for Research in Environmental Sciences, University of Colorado/NOAA, Boulder, CO 80309-0449

BAOSEN LONG

*NOAA/ERL Wave Propagation Laboratory, Boulder, CO 80303**

(Manuscript received 6 August 1984, in final form 21 December 1984)

ABSTRACT

Extratropical cyclogenesis occurs off the east coast of China, over the East China Sea and surrounding areas, as a result of cold-air outbreaks from the mainland about every five days, on the average, during winter months. Many of these storms subsequently propagate northeastward into the Pacific, and in the process they have a substantial impact on the weather of highly populated areas of northeast China, the Koreas and Japan.

This paper presents a climatological analysis of this cyclogenesis for the period 1899–1962 based on U.S. Weather Bureau historical weather maps. The averaged seasonal variability during the period is discussed in some detail with comparisons to sea-surface temperature variability, taken from the Historical Sea Surface Temperature Project data, revealing that the meridional gradient of sea surface temperature across the East China Sea plays a significant role in the annual cycle of cyclogenesis. In contrast, wind speed, air–sea temperature difference and averaged heat fluxes show little relationship to the cyclogenesis. This suggests that the surface baroclinicity associated with this temperature gradient triggers baroclinic instability on the subtropical jet stream as it enters and merges with the Aleutian Low to the east.

Interannual variability of frequency of storm formation is shown to be linked to variations in the surface pressure at Darwin, Australia and, by inference, to the Southern Oscillation. This appears to be a manifestation of the West Pacific teleconnection in which warm equatorial temperatures and anomalous deep convection patterns in the Central Pacific are associated with a deepening and broadening to the west of the Aleutian Low, thus increasing the potential for storm formation over the East China Sea. Variability of storm formation at the frequency of the quasi-biennial oscillation is also suggestive of this mechanism.

1. Introduction

One of the most dramatic manifestations of atmosphere–ocean interaction occurs during wintertime cold-air outbreaks over the warm western boundary currents of the North Pacific and Atlantic Oceans. This phenomenon comprises a mixture of virtually all scales of oceanography and meteorology: the planetary- (or basin-) scale wind-stress curl patterns produce the western boundary current, which interacts with the synoptic-scale weather pattern; as a result, meso- and turbulent-scale phenomena occur in the form of surface-based subsynoptic-scale depressions, cloud streets, enhanced sea states and very large air–sea heat, moisture and momentum fluxes. Frequently, the subsynoptic-scale depressions grow into extratropical cyclones on the synoptic scale. These cold-air outbreaks and the associated air-mass modification have been the subject of several large-scale experimental programs (e.g., the Air Mass Transformation Experiment (AMTEX) as part of the Global Atmospheric Research Program, and, more recently, the Mesoscale Air–Sea Exchange experiment). That synoptic-scale events such as these outbreaks can be the subject of such ambitious field programs is testimony to their ubiquity. They represent an important climatological feature of the east coasts of North America and Asia, and the individual events play a substantial role in coastal and near-coastal island weather. In this paper we discuss a 64-year (1899–1962) climatology of cyclogenesis events over the East China Sea and surrounding regions. Individual events in this area were studied intensively during AMTEX, and analysis and modeling of AMTEX results has greatly improved understanding of the phenomenon. The data and analysis presented here establish a climatological perspective for the East Asian marine cyclogenesis.

In a typical sequence of events leading to this cyclogenesis, a continental synoptic-scale low pressure system propagates north and east across Manchuria and eastern Siberia trailing a cold front across the Yellow Sea and the Korean peninsula. The northerly (or northwesterly) flow behind the front, being extremely dry, as well as cold, presents a very unstable

* Permanent Affiliation: First Institute of Oceanography, National Bureau of Oceanography, Qingdao, Shandong, PRC.

air mass relative to the ocean surface of the East China Sea, which is maintained at ~20°C or more by the Kuroshio Current. If the upper-level trough associated with the original low does not propagate eastward immediately but rather lags in the vicinity of 125°E, the stage is set for the development of a cyclone along the cold front as it passes over the East China Sea. In other cases of cyclogenesis, no cold front is involved; rather, disturbances on a strong northeasterly (subtropical) jet amplify, presumably due to low-level baroclinicity associated with the temperature contrast between the Kuroshio and the continental air to the north. The actual position of the development is crucial to the subsequent weather effects on the populations of East China and Japan. A modeling study of the 13–14 February 1975 AMTEX cyclone by Chen *et al.* (1983) has shown that air–sea heat and moisture fluxes were important factors in the cyclone's development, and that upper-level vorticity advection contributed both to its development and trajectory. We show here that the climatological pattern of cyclone formation in the region is also affected by large-scale tropospheric vorticity patterns and by sea surface temperature (SST) variability. It appears that the West Pacific teleconnection pattern discussed by Wallace and Gutzler (1981) and Horel and Wallace (1981) is manifested in the interannual variations of the frequency of cyclogenesis. Seasonal changes in preferred location of cyclone formation appear to be linked strongly to regional SST variability.

Following a discussion of the data sources and compilation methods in Section 2, we discuss the seasonal variability in Section 3 and the interannual variability in Section 4. Section 5 contains a summary and conclusions.

2. Data sources and methods

a. Cyclogenesis

The formation of extratropical cyclones in the region 120–150°E and 20–40°N was tabulated on a daily basis for the years 1899–1963 by examination of U.S. Weather Bureau historical weather maps (the Daily Synoptic Series—see Hatch, 1983) and compositing the events into 5° squares by month. Each cyclone was counted only once and only with reference to the position of its formation. The criterion used for a cyclone to be counted required a closed isobar to persist for 24 h (2 maps in the series). The analyses that follow use 64 of the 65 years, with the first and last 6 month periods used to provide tails for the year-long running means in some cases. This time period was chosen for two reasons: i) the analysis below uses Fast Fourier Transforms, which operate most efficiently on series that are powers of 2 in length; and ii) we intend this to be a historical climatology, leaving the most recent 20-year period to be analyzed separately as a comparative study. The latter seems justified based on data-network homogeneity considerations.

Figure 1 shows the area studied, with a schematic of the Kuroshio Current streamlines. The annual average of storm formation in the area (Fig. 2) is similar, but not identical, to the wintertime 1932–36 study by Miller and Mantis (1947), who used a similar data extraction technique but higher resolution over a study area displaced approximately 5° to the west and 10° to the north of that used here. The secondary maximum, just southeast of Japan, found by Miller and Mantis is also present in our data during the Fall and Spring. The pattern in Fig. 2 is also consistent with the climatology of more recent years compiled by Whittaker and Horn (1982); minor differences are discussed below. We will concentrate mainly on the primary maximum over the East China Sea in Fig. 2 in our discussion.

b. Related climatology

For analysis of seasonal variability, we use sea surface temperatures, surface air temperatures and wind information from the Historical Sea Surface Temperature Project (HSSTP) (e.g., Fu *et al.*, 1983). This data is comprised of monthly-averaged observations, mostly from ship reports, with 5° resolution. During the period of interest here, there were a large number of missing data points (i.e., 5° square-months), but when the monthly averages are averaged for the period 1899–1959, to construct an average annual cycle, there are no data-void boxes. The minimum number of observations occurs in the northeast corner of the study area, and coverage in the area of primary interest is relatively dense.

The interannual variability is discussed with comparisons to a time series of monthly surface pressure anomalies at Darwin, Australia kindly supplied by E. Rasmusson.

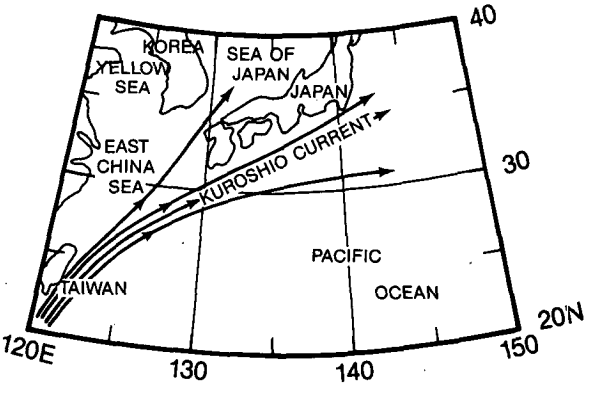

FIG. 1. Study area. Cyclogenesis events from 1899–1962 were composited in 5 degree squares. The Kuroshio Current shown schematically.

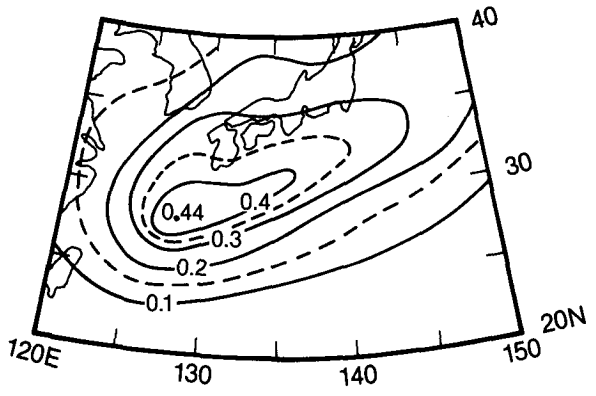

FIG. 2. Average number of events per month per 5 degree square, 1899–1962.

3. Seasonal variability

The annual cycle of storm formation is dominated by the winter months when cold-air outbreaks from the Asian mainland are a frequent occurrence. Figure 3 shows the averaged number of storms per month and the monthly standard deviations for the study area; for comparison, the results of Miller and Mantis (1947) for the winters 1932–36 are also shown (these have been reduced by the ratio of the respective study areas), as is the averaged annual cycle for the years 1958–77 replotted from the Whittaker and Horn (1982) atlas. This seasonal cycle, with a minimum of storm formation in August and a broad Winter–early Spring maximum of a storm forming about every five days, is obviously locked to the Northern Hemisphere seasonality. With the exception of August, the standard deviations for this time period average 2 ± 0.5 storms per month; the Miller and Mantis (1947) results are well within one standard deviation of the longer record. The Whittaker and Horn (1982) annual cycle is also within a standard deviation of the longer record, although differences for the months June–August are somewhat larger than might be expected for a 20-year average. Whether this is due to actual secular variability or to observational network changes is not entirely clear. Whittaker and Horn's data for the region of interest were extracted from the *Mariners' Weather Log,* which is not always consistent with other weather service products. The monthly distributions from the Whittaker and Horn data (not shown) reveal a tendency for more cyclogenesis events in the northeast corner of our study region, particularly in the Spring, than our monthly distributions (Fig. 4).

The monthly distributions in units of storms per month per 5° square (this will be used consistently below) for the period 1899–1962 are shown in Fig. 4. These indicate a shift, during the active seasons, between two relative maxima, one southeast of Japan in the late Fall and late Spring, and one toward the southwest of Japan, over the East China Sea, in the Winter and early Spring. Both maxima overlie the Kuroshio Current, which averages ~20°C during Winter and Spring. The variability of the primary maximum is particularly evident when the mean

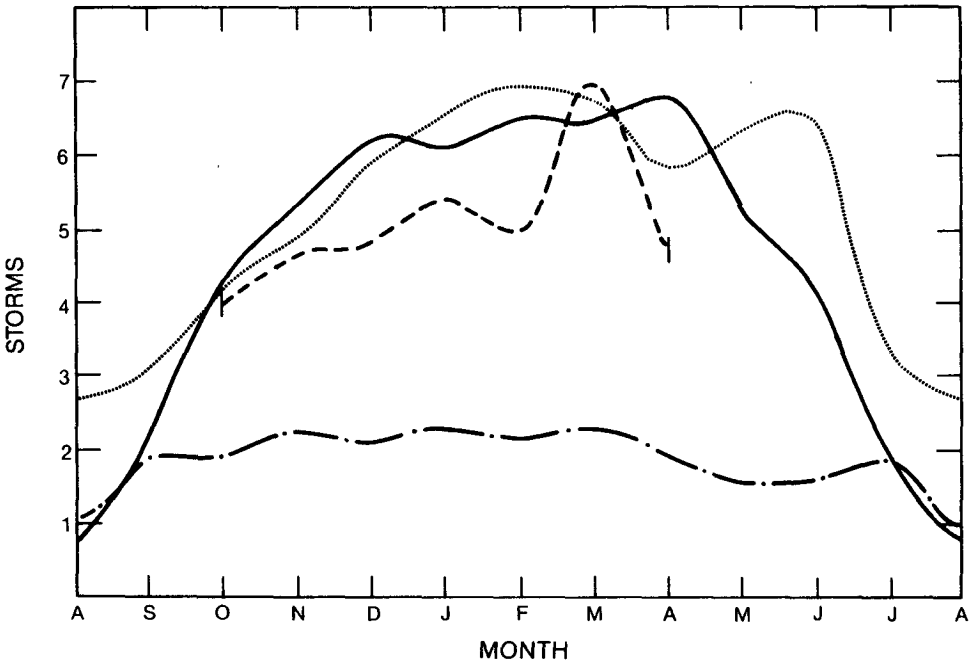

FIG. 3. Average (solid) and standard deviation (dash–dot) of seasonal cycle for entire area, in storms per month. Dashed curve shows results of Miller and Mantis (1947) and dotted curve shows results of Whittaker and Horn (1982) for the area of Fig. 1.

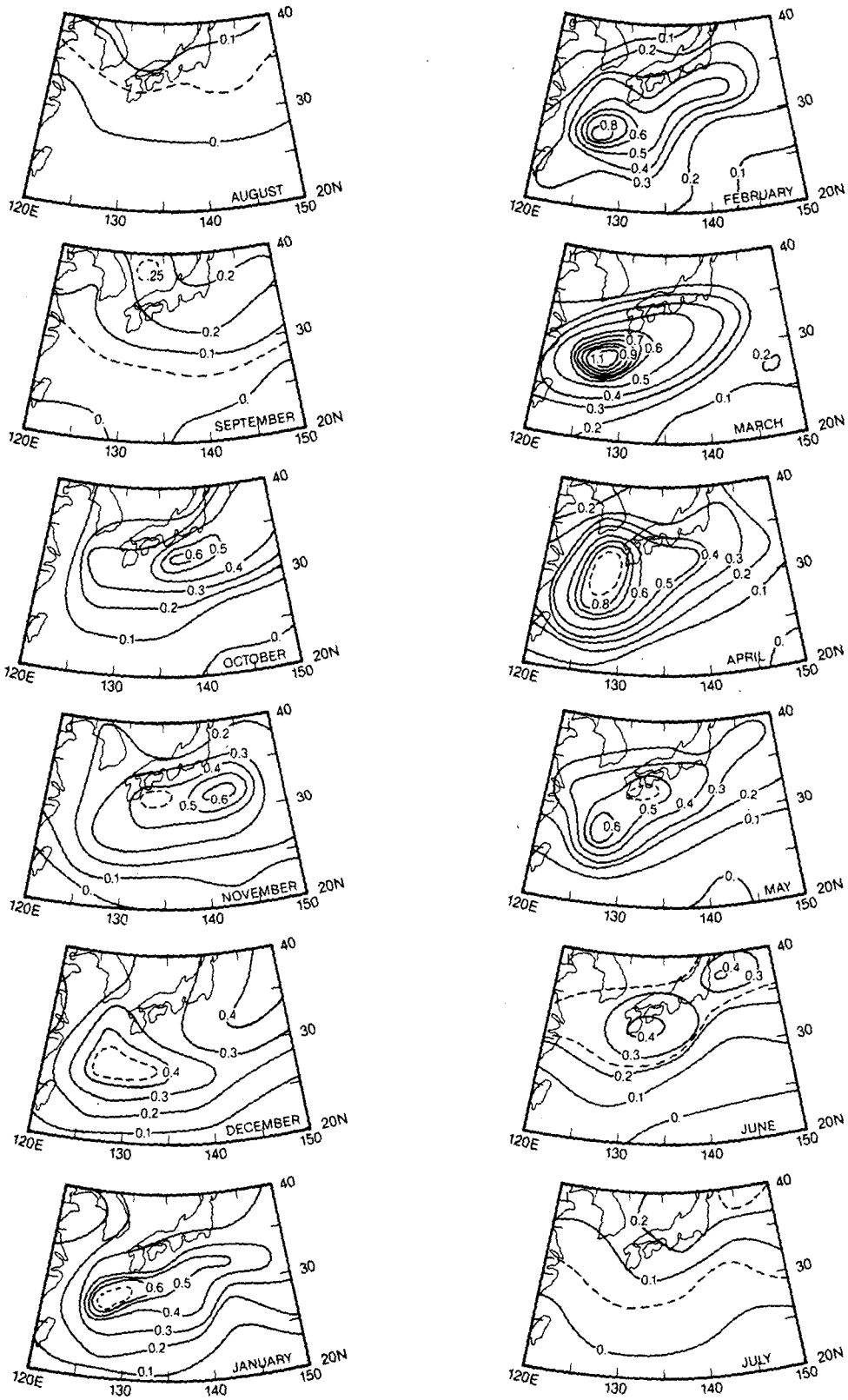

FIG. 4. Average monthly distribution (in storms per month per 5 degree square), August–July.

(Fig. 2) and the first empirical eigenfunction (EOF) (Fig. 5a) are examined together: the rather broad ridge of the maximum averaged cyclogenesis is modulated by strong seasonal variability on its southwest flank. This produces, during the fall months, a secondary maximum southeast of Japan. This east–west variability is also manifested in the second EOF (Fig. 5b), particularly in the Fall when the secondary maximum is strongest, but the much lower percent of variance explained makes the significance of the second EOF relative to the first questionable except during October–January, when the second EOF apparently governs the mean seasonality (Fig. 3). We will restrict our attention here to the annual cycle as manifested in the first EOF (Fig. 5a), and, on the basis of its monthly phase, adopt the convention of years beginning in August, as in Fig. 2, for purposes of the interannual variability analysis.

The annual variability of cyclogenesis shown in Figs. 3, 4 and 5 is obviously most strongly controlled by the overall baroclinicity of the midlatitude westerlies, which is much weaker from July–September than the rest of the year and strongest from January–March (e.g., Oort and Rasmusson, 1971). The position of the strong maximum of the first EOF and its peak in March is less easily explained, however. The occurrence of the maximum downwind of a long northwesterly fetch, across the Yellow and East China Seas (Fig. 1), suggests that accumulation of the surface fluxes during cold-air outbreaks could be the explanation. However, AMTEX modeling results (Chen *et al.*, 1983) suggest that this cannot be considered the sole cause of storm formation, but rather that the storms and fluxes interact: storm development produces strong winds, which enhance surface fluxes, leading to latent heat release, which contributes to storm development, etc, in, perhaps, a CISK-like instability. In seeking an explanation of the seasonal cycle of storms, we use the HSSTP air temperatures, winds and SSTS to investigate potential triggering mechanisms that are consistent with the patterns in Fig. 5a.

The annual average and first EOF of the SST are shown in Fig. 6. Although the details of the Kuroshio are washed out by the averaging, its presence is evident in the southwest–northwest orientation of the isotherms in Fig. 6a between Taiwan and Japan and in the low amplitude of the first EOF to the southeast. The seasonal phase of the first EOF lags the seasonal insolation by ~6 weeks and the largest SST changes

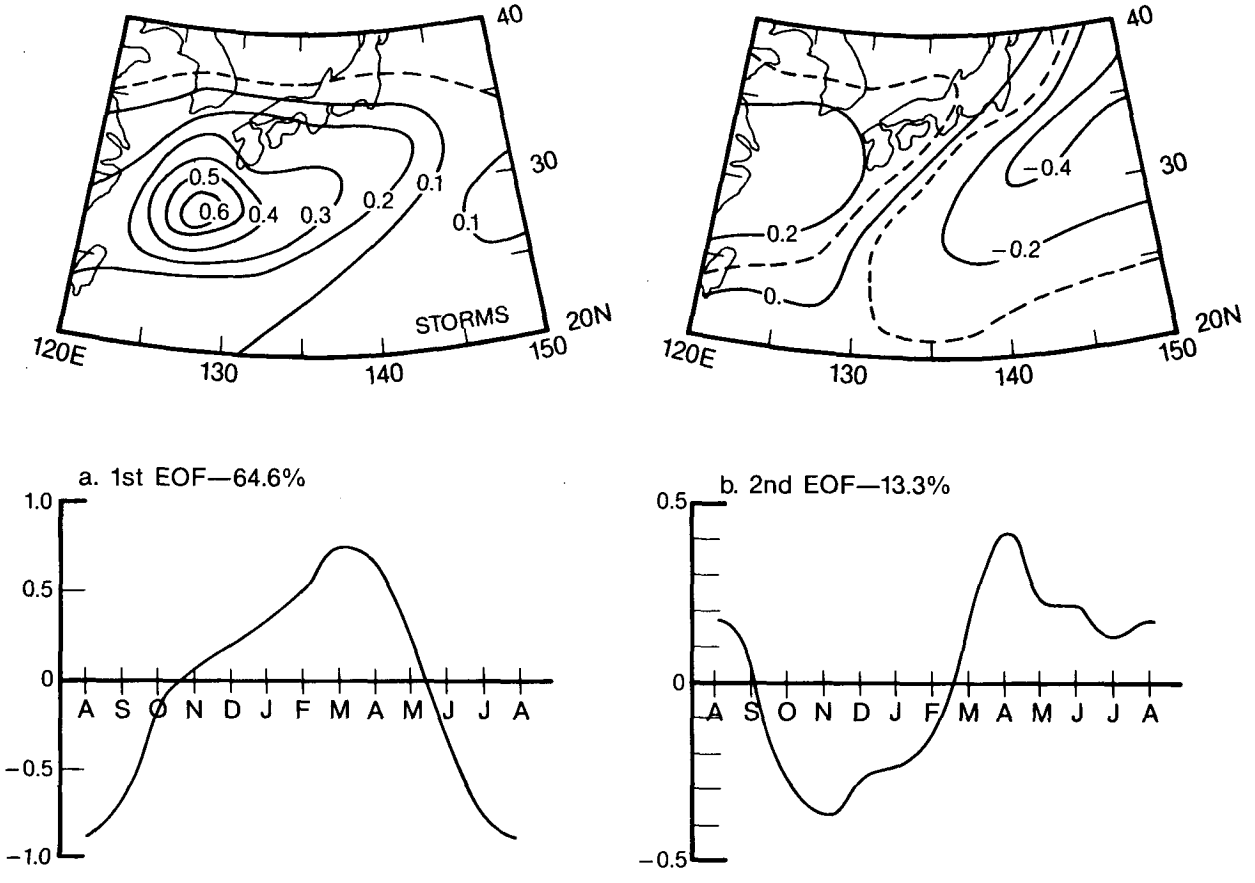

FIG. 5. First (a) and second (b) EOFs of the averaged annual cycle, in storms per month per 5 degree square.

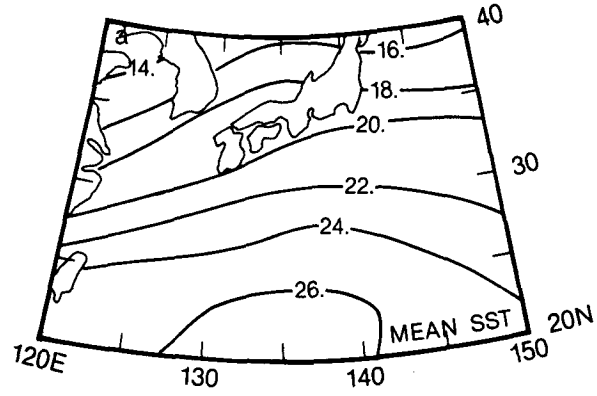

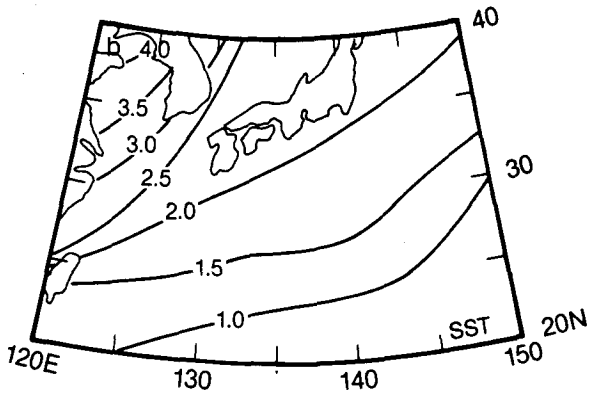

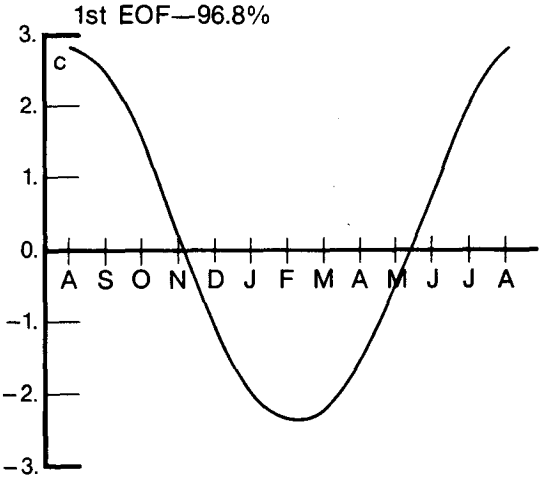

FIG. 6. Average (a) and first EOF (b, c) of SST (°C) from HSSTP.

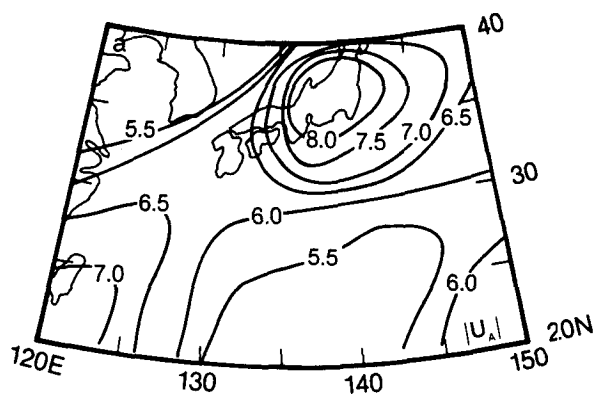

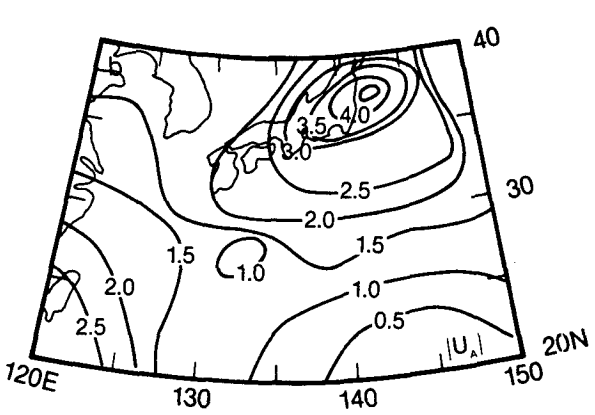

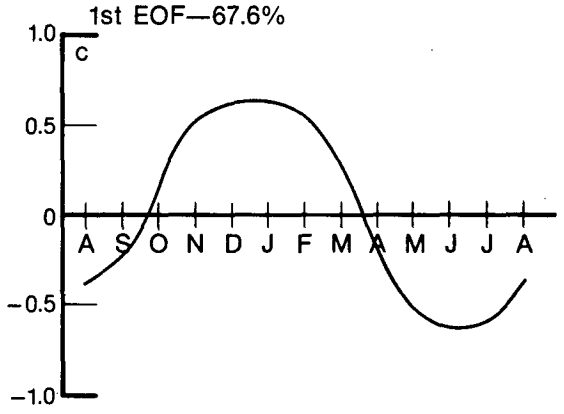

FIG. 7. As in Fig. 6 but for wind speed (m s^{-1}).

occur in the (relatively shallow) Yellow Sea. Comparing Figs. 6b, c with Fig. 5a shows no particular resemblance between the seasonal variability of SST and storms. This is also the case for the wind speed (Figs. 7) and the air–sea temperature difference (Fig. 8). Both of these quantities have annual-average (Figs. 7a, 8a) and first EOF (Figs. 7b, 8b) maxima over Japan, and both have seasonal phases that lead to the first EOF of storm formation by some three months. It is therefore clear that the seasonal variability of heat fluxes, as implied by the product of the first EOFs in Figs. 7 and 8, has little relationship with storm variability. (Submonthly-scale correlations of wind and temperature and the fact that the HSSTP data do not correspond precisely to the storm data, are neglected here, as discussed in Section 2b. The differences discussed above, however, are so large that the conclusion is unlikely to be changed by a better dataset.)

As shown by the modeling study of Chen *et al.*

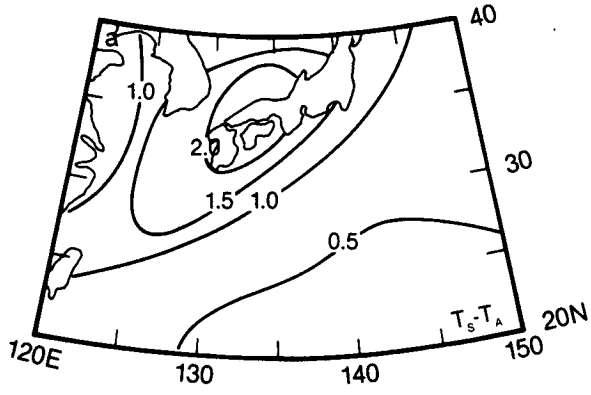

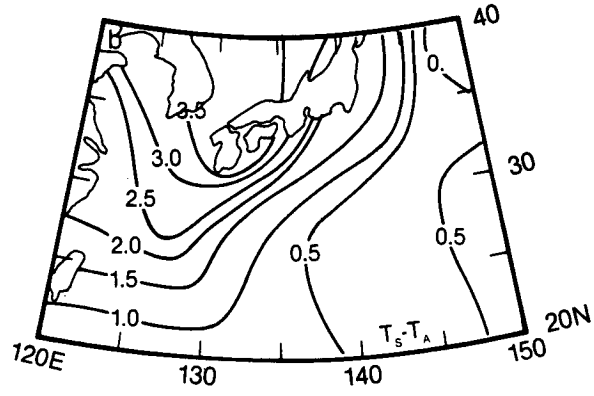

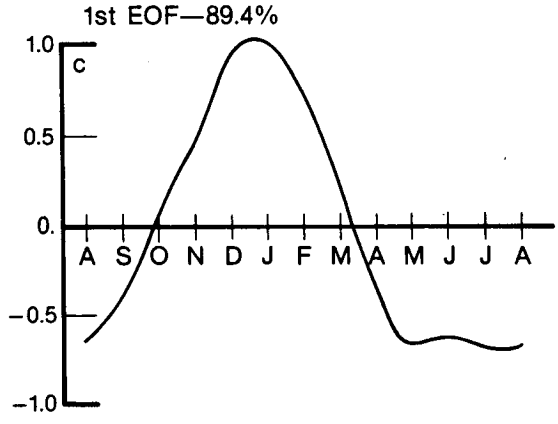

FIG. 8. As in Fig. 6 but for air–sea temperature difference (°C).

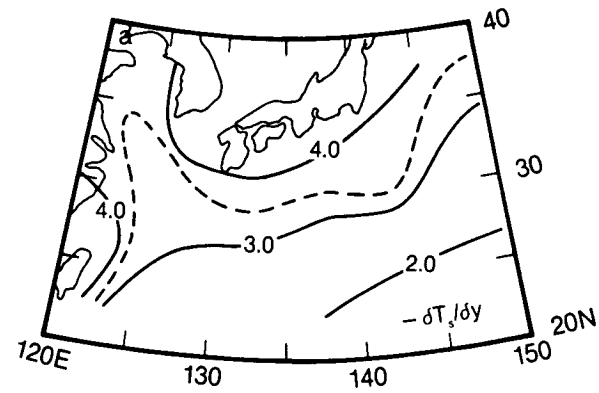

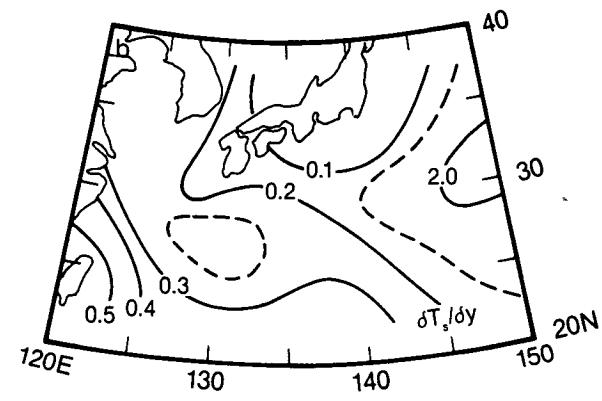

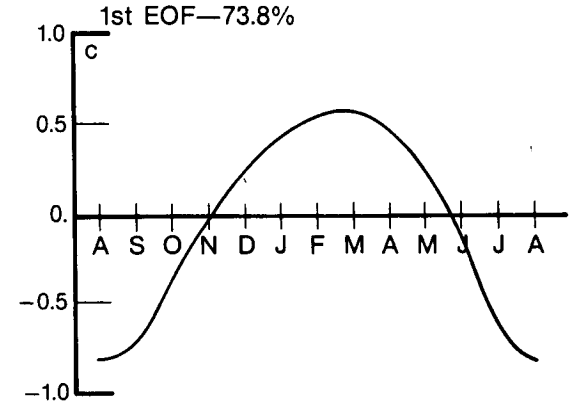

FIG. 9. As in Fig. 6 but for meridional SST gradient (°C/5 deg).

(1983), it seems clear that latent heat release in the lower atmosphere is an important mechanism for development of surface depressions into the extratropical cyclones tabulated in the present study. It appears from the present data, however, that the initial position of storm formation is controlled by baroclinic instability processes. Figure 9 shows the annual mean and first EOF of the north–south SST gradient (in °C/5° Lat.). Meridional surface temperature gradients play a key role in baroclinic instability theory by relaxing the necessary condition for instability and allowing instabilities in an otherwise stable flow (e.g., Gill, 1982, Section 13.5). Figure 10 gives the correlation coefficients of the annual cycles of this gradient and the storm formation, with 95% or higher t-test significance levels shaded. (The time series have also been analyzed using the autocorrelation functions to determine the effective number of degrees of freedom by the technique of Davis (1976); this accounts for the variability of the 95% significance

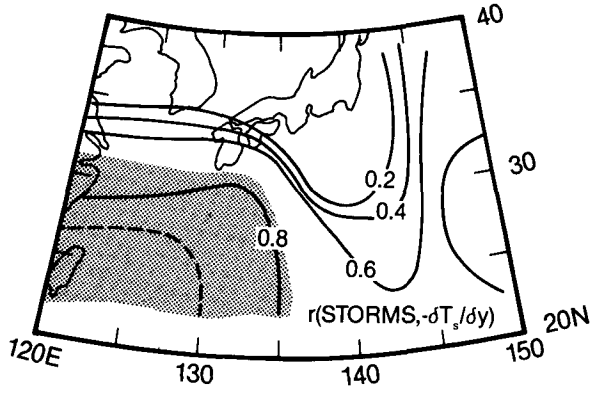

FIG. 10. Point-by-point correlation coefficients of averaged annual cycles of storm formation and meridional SST gradient. Shaded area denotes 95% or greater significance.

limit.) Significance is confined to the southwest corner of the analysis domain, and the maximum of the first storm EOF corresponds to a strong ridge of maximum SST gradient; the time coefficients are almost precisely in phase. This is of interest here because no other quantity, including temperature advection, the SST gradient in the direction of the wind, the heat flux gradient in any direction and several other even less physical parameters, comes even close to the correlations in Fig. 10. We conclude that the surface baroclinicity induced by the strong February–April SST gradients across the Yellow and East China Seas controls, to a large degree, the seasonal changes of the position of maximum storm formation.

The fall–winter east–west variability manifested in the second EOF (Fig. 5b) has no such obvious explanation that we have been able to find with the data set used here. We speculate that it is related to shifts in the position and strength of the Aleutian Low at 500 mb and are in the process of examining this further.

4. Interannual variability

The results discussed in Section 3 suggest that a monthly time series of the interannual variability of storm formation would be dominated by the strong seasonal cycle (the peak-to-peak April–August difference in Fig. 2 is ~6 storms per month). The 1899–1962 (reckoning years beginning in August) time series of yearly-averaged storm formation, in units of storms per month, in Fig. 11 bears this out, showing a peak-to-peak change of somewhat more than three storms per month between the most and least active years. Moreover, the standard deviation of the annual data shown in Fig. 11 is about one-half the standard deviation of the monthly data. Thus, the time-series analyses reported in this section have been made using series that were smoothed with a year-long running-average filter.

Figure 11 exhibits substantial short-period variability on the 2–3 year time scale. For example, during the decade of the 1930s and during the middle 1950s the year-to-year changes dominated the two-year trends, whereas before ~1930, this short-period variability appears to be somewhat slower. There is also the suggestion of a 20–30 year periodicity, although the series is clearly not long enough to be certain about this. From the perspective of time-series

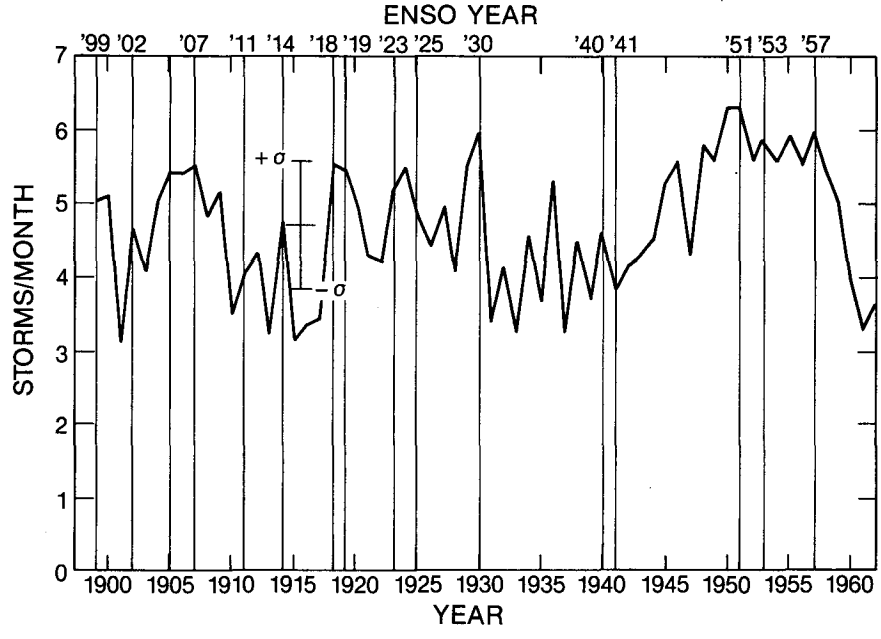

FIG. 11. Annual average (August–July) of storm formation for study area, 1899–1962. Thin vertical lines correspond to ENSO years, from Rasmusson and Wallace (1983).

analysis, these periodicities are difficult to analyze. The two-year periodicity occurs at the Nyquist frequency, and the very long periods are apt to be analyzed incorrectly because of nonstationarity. The mean distributions of storm formation for the four quarters of the period analyzed show significant variability, but the major patterns are common: the ridge of maximum storm formation running southwest–northeast along the southeast flank of Japan, with the maximum area over the Kuroshio in the East China Sea to the southwest of Japan. Table 1 gives averages and standard deviations for the four periods; as is clear from Fig. 11, the third period (1931–46) was the least active, and the last period was the most active, with a difference of about 21% of the overall mean. It is interesting that the data from 1958–77 presented by Whittaker and Horn (1982) shows about the same number of storms per month (5.29) as the period 1947–62. Therefore, the possibility that the post-WW II increases in the observing network have had an influence on the "climatology" cannot be ruled out.

Despite these less-than-ideal factors, a spectral analysis of the data in Fig. 11 gives a significant, and interesting, spectral peak at ~5⅓ years. This was found by Fast Fourier Transforming (FFT) a time series of "pseudomonthly" values of storm formation, where a "pseudomonth" (p-month) is ~6.5 weeks; i.e., there are 8 p-months per year. (FFT routines commonly pad time series to make them a power of 2 in length; our analysis of 64 years at 8 p-months per year thus needed no "padding" and no spurious low-frequency power, beyond that due to the nonstationarity discussed above, appears.) Since the storm data, as originally analyzed, was composited monthly, we constructed the p-month series using the expedient of halving every other month rather than reanalyzing the original data. Thus, p-month 1 is the sum of the August value and half the September value, and so forth. This approach to the spectral analysis also increases the Nyquist frequency to (3 months)$^{-1}$ and puts the 2–3 year variability mentioned previously into a well-resolved part of the spectrum.

Figure 12 shows the FFT-generated power spectrum of the p-month series on an energy-proportional plot, in which the bandwidth/confidence crosses are valid only at the peaks where they appear. Two bands of significant power appear (besides the low-frequency effects of nonstationarity discussed above): a band from (8 yr)$^{-1}$ to ~(3 yr)$^{-1}$ and a band from (3 yr)$^{-1}$ to ~(1.7 yr)$^{-1}$. The lower-frequency band is centered

TABLE 1. Yearly averages and standard deviations (storms per month).

	1899–1962	1899–1914	1915–30	1931–46	1947–62
Average	4.71	4.58	4.73	4.26	5.28
σ	0.88	0.75	0.81	0.70	0.92

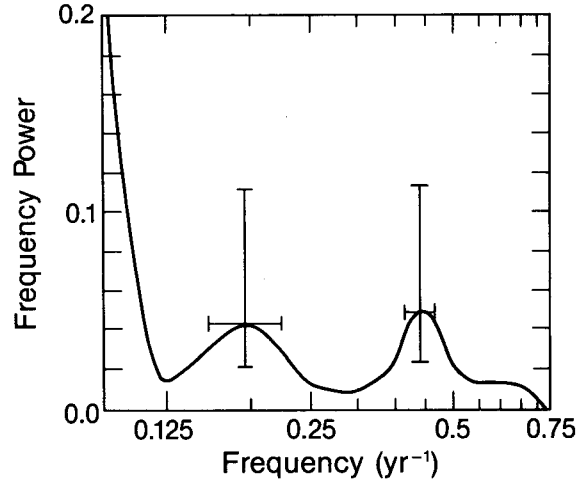

FIG. 12. Energy-proportional FFT spectrum of interannual storm variability with 95% confidence interval and bandwidth shown for the two peaks.

at (5⅓ yr)$^{-1}$, and is somewhat broader and contains more power than the higher-frequency band, which is associated with the 2–3 year variability that appears in Fig. 11.

The appearance of spectral power of East Asian cyclogenesis in the 5-year band in Fig. 12 can be explained, we assert, by the West Pacific teleconnection discussed by Wallace and Gutzler (1981) and Horel and Wallace (1981). Figures 9b and 9c of the latter paper present correlation coefficients between the convective rainfall at Fanning Island in the central equatorial Pacific and the Southern Oscillation Index (SOI), respectively, and 700 mb Northern Hemisphere geopotential heights. The West Pacific teleconnection is manifested as a correlation between high rainfall and low SOIs, and a deep Aleutian Low that is also broadened toward the west. It is straightforward to conclude that this anomalous troughing during El Niño/Southern Oscillation (ENSO) episodes would tend to lead to more baroclinic activity in the far western Pacific, all other things being equal. The thin vertical lines, with the scale at the top in Fig. 11 show ENSO years, as defined by Rasmusson and Wallace (1983), for the time period analyzed here. There is a tendency for ENSO years to coincide with local maxima of storm formation, although there also a number of years (e.g., 1911, 1941) when this clearly does not happen.

Figure 13 shows FFT spectra of Darwin, Australia surface pressure anomalies (DSPA) (for which p-months were generated from a monthly series), which station is commonly used in formulating an SOI (e.g., Trenberth, 1984). The only statistically significant spectral peak in Fig. 13 occurs at (5.3 yr)$^{-1}$; the DSPA time series also contains low-frequency (nonstationary) power similar to the storm data in Fig. 12. To compare the storm data with the Darwin pressure record, we first subjected both p-month time series to a high-pass filter with a cutoff at (8 yr)$^{-1}$ in

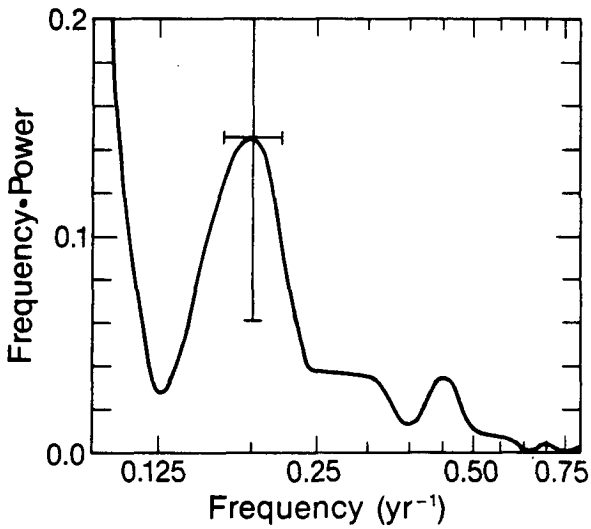

FIG. 13. FFT spectrum of Darwin surface pressure anomalies.

order to filter the nonstationarity from each record. The cross spectrum of the high-pass-filtered time series of the storm formation and the DSPA is shown in Fig. 14; the spectrum is dominated by the peak at $(5\frac{1}{3}\ \mathrm{yr})^{-1}$, for which the DSPA leads by about two months. Correlation coefficients for these two series are significant at the 95% level for DSPA leading by 0, 1 and 2 p-months, with the maximum correlation (0.346) at 1 p-month (1.5 months). The conclusion that the variations in storm formation and the DSPA (and therefore the SOI) are related thus seems foregone. The lag of the storm formation behind the DSPA (and SOI) is not quite as easily explained, but can perhaps be attributed to the relationship of changes in convective rainfall patterns in the equatorial Pacific during ENSO events to midlatitude teleconnections. If these convective rainfall anomalies induce a midlatitude response, whether through the hypothesized waveguide mechanism (Hoskins and Karoly, 1981), or through another, unexplained mechanism, it would be expected that this response would lag SOI changes by slightly longer than do the rainfall anomalies, and a lag of 1–3 months for changes in cyclogenesis associated with altered long-wave patterns is not unreasonable.

A reviewer has suggested that the other significant peak in the storm-data spectrum (Fig. 12) at $\sim(2.3\ \mathrm{yr})^{-1}$ may be indicative of the quasi-biennial oscillation (QBO). The recent analysis of 55 years of Northern Hemisphere sea-level pressure data (Trenberth and Shin, 1984), using a band-pass filter centered on 26 months, indicates that variability of the Aleutian Low is the dominant signal of the QBO. Although the second spectral peak in Fig. 12 is centered at $(27\ \mathrm{months})^{-1}$, the uncertainty of the FFT analysis makes this a clear possibility. In particular, the same mechanism, i.e., that deepening and broadening toward the west of the Aleutian Low and its upper-level trough would increase the potential for baroclinic instability in the West Pacific region, could explain the SOI and QBO connections to the storm variability.

A final variation of interest is shown in Fig. 15. The seasonal variability for the 16 ENSO years indicated in Fig. 11, and for the strongest eight of those years, is contrasted to that for all years and for all non-ENSO years. (Recall that the standard deviation for all months but August is approximately 2 storms per month.) The tendency for earlier and more frequent storm formation during ENSO years is apparent, and is stronger for the eight strongest events. This result at first suggested to us that a potential for seasonal forecasts might be indicated. However, when we examined the storm formation for the more recent ENSO episodes of 1969, 1972 and 1982, the variability shown in Fig. 15 did not hold. Although there was a significantly greater number of storms during those years, the maximum frequency occurred during March and April rather than December and January as in Fig. 15. Thus, while it cannot be stated that ENSO years produce an earlier maximum, it is very likely to be stronger.

5. Summary and conclusion

By examination of U.S. Weather Bureau historical weather maps, we have produced a climatology of extratropical marine cyclogenesis that occurs over the East China Sea and surrounding areas. Seasonal and interannual analyses of this climatology show:

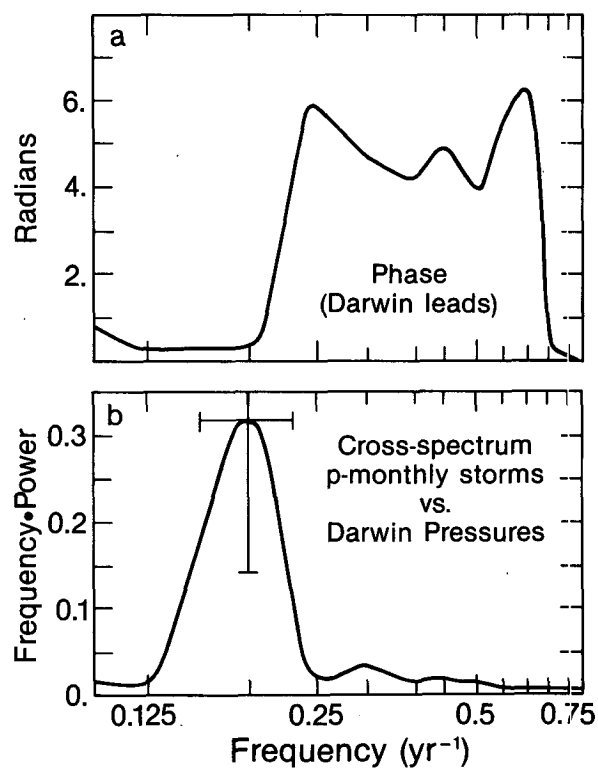

FIG. 14. Phase (a) and amplitude (b) of cross-spectrum of high-pass-filtered storm series and Darwin pressure anomaly series.

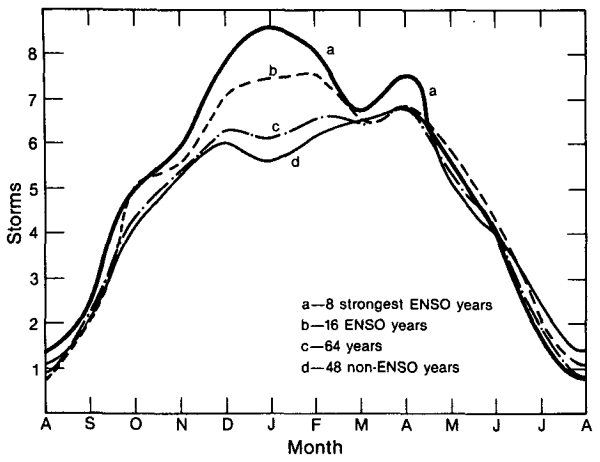

FIG. 15. Averaged seasonal cycle during strong ENSO years (curve a); all ENSO years in Fig. 11 (curve b); all years (from Fig. 3-curve c); and non-ENSO years (curve d).

• The seasonal variability of storm formation is locked to the large-scale baroclinicity, with a minimum in August and a rather broad maximum from December–April, during which time a storm forms about every 5 days.

• The area of maximum formation is over the East China Sea to the southwest of Japan; a secondary maximum appears over the Kuroshio just southeast of Japan. The trajectory of the storms (generally to the northeast) thus implies a dramatic influence on Japan's weather.

• While the gross features of the seasonal variability are easily explained, the details of these maxima are not. The results presented here indicate that the wintertime maximum to the southwest of Japan results from the strong meridional SST gradient across the Yellow and East China Seas—i.e., the surface baroclinicity—rather than the SST itself. This mechanism of air–sea interaction should be investigated further.

• The interannual variability of frequency of storm formation is strongly linked to the large-scale tropical variability of the Southern Oscillation, with the likely mechanism being the West Pacific teleconnection pattern. During ENSO events the frequency of storm formation can increase by as much as 20% over "normal" years.

• The possibility of a link between interannual variability of storm formation and the quasi-biennial oscillation, through a dynamical mechanism similar to that of the West Pacific teleconnection, also exists.

This study can, in some ways, be viewed as a pilot project, in that a number of questions remain and more analysis is indicated. For example, it would be of interest to examine storm trajectory variability on all time scales, and storm strength and duration. A correlation analysis with 500 mb (or 700 mb) height-field variability would be useful to confirm (or rebut) the teleconnection arguments we have presented, and cross-analyses with equatorial SSTs would also by useful. Since coastal cyclogenesis also occurs over the Gulf Stream, a similar study for the Eastern United States would be of interest. Finally there remains the difficult problem of explaining the teleconnections in terms of a theory (or model) that consistently produces realistic results above the noise level, as are observed.

Acknowledgments. We would like to express our appreciation to the Scientific Exchange Program between NOAA and the National Bureau of Oceanography of the PRC for the opportunity to work together, and to A. S. Frisch of NOAA/ERL/WPL for facilitating this exchange. HPH is supported by the National Science Foundation via Grant ATM 82-09115 and by NOAA through the Equatorial Pacific Ocean Climate Studies program. We thank E. J. Steiner for assistance with EOF analysis, R. Slutz and S. Woodruff for the HSSTP data and associated software, G. K. Greenhut for critical comments on the manuscript and an anonymous reviewer for bringing the Whittaker and Horn (1982) atlas to our attention.

REFERENCES

Chen, T.-C., C.-B. Chang and D. J. Perkey, 1983: Numerical study of an AMTEX 75 oceanic cyclone. *Mon. Wea. Rev.*, **111**, 1818–1829.

Davis, R. E., 1976: Predictability of sea surface temperature and sea level pressure anomalies over the North Pacific. *J. Phys. Oceanogr.*, **6**, 249–266.

Fu, C., J. Fletcher and R. Slutz, 1983: The structure of the Asian monsoon surface wind field over the ocean. *J. Climate Appl. Meteor.*, **22**, 1242–1252.

Gill, A. E., 1982: *Atmosphere–Ocean Dynamics.* Academic Press, 662 pp.

Hatch, W. C., 1983: *Selective Guide to Climatic Data Sources,* KMRD No. 4.11, NOAA/NCDC, Asheville. [Available from the Superintendent of Documents, U.S. Government Printing Office, Washington, DC 20402; stock No. 643-153/359.]

Horel, J. D., and J. M. Wallace, 1981: Planetary-scale atmospheric phenomena associated with the Southern Oscillation. *Mon. Wea. Rev.*, **109**, 813–829.

Hoskins, B. J., and D. A. Karoly, 1981: The steady linear response of a spherical atmosphere to thermal and orographic forcing. *J. Atmos. Sci.*, **38**, 1179–1196.

Miller, J. E., and H. T. Mantis, 1947: Extratropical cyclogenesis in the Pacific coastal region of Asia. *J. Meteor.*, **4**, 29–34.

Oort, A. H., and E. M. Rasmusson, 1971: *Atmospheric Circulation Statistics.* NOAA Prof. Paper 5, 323 pp. [Available from the Superintendent of Documents, U.S. Government Printing Office, Washington, D.C. 20402; stock No. 0317-0045.]

Rasmusson, E. M., and J. M. Wallace, 1983: Meteorological aspects of the El Niño/Southern Oscillation. *Science,* **222**, 1195–1202.

Trenberth, K. E., 1984: Signal versus noise in the Southern Oscillation. *Mon. Wea. Rev.*, **112**, 325–332.

——, and W.-T. K. Shin, 1984: Quasi-biennial fluctuations in sea level pressures over the Northern Hemisphere. *Mon. Wea. Rev.*, **112**, 761–777.

Wallace, J. M., and D. S. Gutzler, 1981: Teleconnections in the geopotential height field during the Northern Hemisphere winter. *Mon. Wea. Rev.*, **109**, 784–812.

Whittaker, L. M., and L. J. Horn, 1982: *Atlas of Northern Hemisphere Extratropical Cyclone Activity, 1958–1977.* Rep. UWMETW 1-82/1, University of Wisconsin-Madison, 70 pp. [ISSN No. PB83-225722.]